Cellular Physiology and Biochemistry

Cell Physiol Biochem 2018;48:2409-2428
DOI: 10.1159/000492656
Published online: 15 August, 2018
Accepted: 6 August, 2018

Original Paper

Crucial Roles of 5-HT and 5-HT$_2$ Receptor in Diabetes-Related Lipid Accumulation and Pro-Inflammatory Cytokine Generation in Hepatocytes

Jihua Fu[a] Chen Li[b] Guangli Zhang[b] Xin Tong[b] Haiwei Zhang[b] Jie Ding[b] Yingying Ma[b] Ru Cheng[b] Shanshan Hou[b] Shanshan An[b] Xin Li[b] Shaoxin Ma[b]

[a]Department of Physiology, China Pharmaceutical University, Nanjing, [b]Laboratory of Cardiovascular Pharmacology, China Pharmaceutical University, Nanjing, China

Key Words
5-HT synthesis • 5-HT$_2$ receptor • Protein kinase C epsilon • 5-HT degradation • Monoamine oxidase A • Diabetic hepatic disease

Abstract
Background/Aims: Previously, we confirmed that liver-synthesized 5-HT rather than non-liver 5-HT, acting on the 5-HT$_2$ receptor (5-HT$_2$R), modulates lipid-induced excessive lipid synthesis (ELS). Here, we further revealed the effects of the hepatocellular 5-HT system in diabetes-related disorders. ***Methods:*** Studies were conducted in male ICR mice, human HepG2 cells, and primary mouse hepatocytes (PMHs) under gene or chemical inhibition of the 5-HT system, key lipid metabolism, and inflammation-related factors. Protein and messenger RNA expression and levels of the factors were determined via western blotting, reverse transcription PCR, and quantitative assay kits, respectively. Hepatic steatosis with inflammation and fibrosis, intracellular lipid droplet accumulation (LDA), and reactive oxygen species (ROS) location were determined via hematoxylin and eosin, Masson's trichrome, Oil red O, and fluorescent-specific staining, respectively. ***Results:*** Palmitic acid induced the activation of the 5-HT system: the activation of 5-HT$_2$R, primarily 5-HT$_{2A}$R, in addition to upregulating monoamine oxidase A (MAO-A) expression and 5-HT synthesis, by activating the G protein/phospholipase C pathway modulated PKCε activation, resulting in ELS with LDA; the activation of NF-κB, which mediates the generation of pro-inflammatory cytokines, was primarily due to ROS generation in the mitochondria induced by MAO-A–catalyzed 5-HT degradation, and secondarily due to the activation of PKCε. These effects of the 5-HT system were also detected in palmitic acid- or high glucose-treated PMHs and regulated multiple inflammatory signaling pathways. In diabetic mice, co-treatment with antagonists of both 5-HT synthesis and 5-HT$_2$R

C. Li, G. Zhang, X. Tong, H. Zhang, J. Ding and Y. Ma contributed equally to this work.

Jihua Fu, PhD
Department of Physiology, China Pharmaceutical University
639 Long Mian Road, 211198, Nanjing, Jiangsu (China)
E-Mail jihua_fu@cpu.edu.cn

significantly abolished hepatic steatosis, inflammation, and fibrosis as well as hyperglycemia and dyslipidemia. ***Conclusion:*** Activation of the hepatocellular 5-HT system plays a crucial role in inducing diabetes-related hepatic dysfunction and is a potential therapeutic target.

Introduction

Non-alcoholic fatty liver disease (NAFLD) is one of the most prevalent liver diseases worldwide, which progresses from simple steatosis to inflammatory non-alcoholic steatohepatitis (NASH) and in some cases even to cirrhosis or hepatocellular carcinoma [1]. NAFLD is strongly associated with type 2 diabetes mellitus (T2DM) [2]. In NAFLD, excessive lipid synthesis (ELS) occurs in the liver, mainly including *de novo* lipogenesis and triacylglycerol (TG) and very low-density lipoprotein (VLDL) syntheses, resulting in lipid accumulation (hepatic steatosis) and increased VLDL secretion to the blood. In general, the development of an NAFLD lesion is a consequence of high dietary fat intake and/or increased lipolysis in adipose tissue with a high level of free fatty acids (FFAs) in the blood [3]. Hepatic steatosis and inflammation in NAFLD are believed to contribute to insulin resistance (IR) [4]. However, the pathogenesis of NAFLD is still unclear [5].

Serotonin (5-hydroxytryptamine, 5-HT) is synthesized from L-tryptophan by tryptophan hydroxylase (Tph) and aromatic amino acid decarboxylase (AADC). There are two Tph subtypes found centrally (Tph2) and peripherally (Tph1) [6]. The degradation of 5-HT is mainly catalyzed by mitochondrial monoamine oxidase A (MAO-A) [7], generating 5-hydroxyindolic acid and reactive oxygen species (ROS), primarily H_2O_2 [7]. In addition to its role as a neurotransmitter in the regulation of central nervous system function, 5-HT also has multiple physiological functions in the periphery [8, 9]. The action of 5-HT depends on the 5-HT receptor, which includes 7 families (types 1–7 5-HT receptor) [10]. The 5-HT_2 receptor (5-HT_2R), which includes the subtypes 5-HT_{2A}R, 5-HT_{2B}R, and 5-HT_{2C}R, is distributed in multiple organs, such as the stomach, intestine, heart, kidney, and adipose tissue [11]. The liver has a distribution of 5-HT_{2A}R and 5-HT_{2B}R. We previously found that hepatocytes also synthesize 5-HT, which acts on 5-HT_2R to play a pivotal role in multiple cause-induced hepatic steatosis and systemic IR with dyslipidemia and hyperglycemia, such as caused by long-term stress [12], glucocorticoids [13], and a high-fat diet (HFD) [14] in rats. Saturated fatty acid (SFA)-induced lipid synthesis with lipid droplet accumulation (LDA) in hepatocytes is also closely correlated with increased 5-HT synthesis and 5-HT_2R activation [14]. The activation of 5-HT_2R can mediate mammalian target of rapamycin (mTOR) activation in hepatocytes [12, 14]. Several investigations have also revealed the relationship between the peripheral 5-HT system and some diseases, including NAFLD and T2DM [15, 16]. However, the mechanism by which the peripheral 5-HT system modulates T2DM-related metabolic dysfunction remains unclear.

Recently, we found that 5-HT system activation with increased 5-HT synthesis and activated 5-HT_2R plays a crucial role in the etiology of diabetic liver disease, resulting in protein kinase C epsilon (PKCε) activation with ELS, oxidative stress with the activation of nuclear factor κB (NF-κB) and multiple inflammatory signaling molecules, and pro-inflammatory cytokine generation (PICG) in hepatocytes, which are implicated in the effects of SFA and high glucose (HG). In this study, we treated HepG2 cells and primary mouse hepatocytes (PMHs) with palmitic acid (PA) or HG as an *in vitro* study; an HFD-fed and streptozotocin (STZ)-induced T2DM mouse model was established, and the mice were treated with or without an AADC and 5-HT_2R inhibitor (alone or in combination) to confirm the therapeutic effects of inhibiting the peripheral 5-HT system on T2DM with NASH.

Materials and Methods

Materials

The following primary antibodies were used: anti-5-HT_{2A}R and anti-5-HT_{2B}R were purchased from Santa Cruz Biotechnology (Santa Cruz, CA); anti-Tph1, anti-AADC, anti-MAO-A, anti-glycerol-3-phosphate acyltransferase 1 (GPAT1), anti-microsomal triglyceride transfer protein (MTTP), anti-lamin-B1, anti-IκBα, anti-NF-κB p65, anti-PI3K p85, anti-Akt, anti-phospho-Akt (Ser^{473}), anti-p38, anti-phospho-p38 (Thr^{180}/Tyr^{182}), anti-c-Jun N-terminal kinase (JNK), anti-phospho-JNK (Thr^{183}/Tyr^{185}), anti-mTOR, anti-phospho-mTOR (Ser^{2448}), anti-extracellular-signal regulated kinase 1/2 (ERK1/2), and anti-phospho-ERK1/2 (Thr^{202}/Tyr^{204}) were from Signalway Antibody (College Park, MD); anti-PKCε and anti-β-actin were from Bioworld Technology (St Louis Park, MN); anti-Na^+-K^+-ATPase, anti-G protein α_q ($G\alpha_q$), and anti-acetyl-CoA carboxylase (ACC) were from Abcam (Cambridge, UK); and anti-signal transducer and activator of transcription 3 (STAT3) and anti-phospho-STAT3 (Tyr^{705}) were from Cell Signaling Technology (Danvers, MA). Triacsin C, U-73122, para-chlorophenylalanine (pCPA), and sarpogrelate HCl (Sar, used in cell experiments) were from ApexBio Technology LLC (Houston, TX). Carbidopa (CDP) and Sar tablets (used in animal experiment) were from Mitsubishi Tanabe Pharma (Tokyo, Japan) and Tokyo Chemical Industry (Tokyo, Japan), respectively. Clorgiline (CGN), saponin, D-glucose, PA, phorbol 12-myristate 13-acetate, STZ, fluoxetine (Flx), and amobarbital sodium were from Sigma-Aldrich (St. Louis, MO). Fetal bovine serum (FBS) was from Zhejiang Tianhang Biotechnology (Hangzhou, China). 5-HT was from Alfa Aesar (Lancashire, UK). PKCε inhibitor peptide (PIP) was from Santa Cruz Biotechnology. Dulbecco's modified Eagle's medium (DMEM) and Williams E medium were from Gibco (Gaithersburg, MD). Entanster™-H4000 was from Engreen Biosystem (Beijing, China). DCFH-DA, Enhanced BCA Protein Assay Kit, and Cell Lysis Buffer for western blotting were from Beyotime (Shanghai, China). MitoTracker® Red CMXRos was purchased from Yeasen (Shanghai, China). Assay kits for tissue and cell TG, H_2O_2, and malondialdehyde (MDA), and for serum alanine aminotransferase (ALT), aspartate aminotransferase (AST), glucose, FFAs, low-density lipoprotein cholesterol (LDL-c), high-density lipoprotein cholesterol (HDL-c), and TG were from Nanjing Jiancheng Bioengineering Institute (Nanjing, China). Mouse or human enzyme-linked immunosorbent assay (ELISA) kits for insulin, VLDL, 5-HT, human tumor necrosis factor alpha (TNF-α), interleukin 1 beta (IL-1β), diacylglycerol (DAG), inositol triphosphate (IP3), L-dopamine, hydroxyproline, and IL-6 were from ShangHai HengYuan Biological Technology (Shanghai, China). Protein extraction kits for nuclear, cytoplasmic, and plasmalemma proteins were from KeyGEN BioTECH (Nanjing, China).

Establishment of T2DM model and drug treatment

ICR male mice (6–8 weeks old), purchased from B&K Universal Group Ltd. (Shanghai, China), were handled in accordance with institutional procedures and approved by the Laboratory Animal Care Committee at China Pharmaceutical University. The mice were housed on a 12-h light/dark cycle with access to water and food *ad libitum*. The T2DM mouse model was established according to Luo et al [17]. with modifications. Briefly, mice fed an HFD (consisting of 16% [w/w] protein, ≥28% carbohydrates, 29.5% fat, 3.6% cholesterol) for 4 weeks were injected intraperitoneally with STZ (80 mg/kg). At 72 h after STZ injection, fasting blood glucose (FBG, the mice were fasted for 14 h) was tested via tail vein blood, and those with FBG ≥ 11.1 mol/L were considered as T2DM mice.

Since Tph1 inhibitors show low oral bioavailability, such as pCPA and LP533401 [15], we chose the AADC inhibitor CDP, which has high oral bioavailability, to inhibit peripheral 5-HT synthesis. All T2DM mice were divided randomly into 4 groups as well as control (Ctrl) mice (N = 8 per group): Ctrl mice were fed regular chow; HFD-fed T2DM mice were treated with or without Sar, a 5-HT_2R inhibitor, CDP, and a combination of Sar and CDP (Sar:CDP = 2:1), respectively. The Ctrl and T2DM mice without drug treatment were orally administered 0.5% CMC-Na, the vehicle used to dissolve Sar and CDP, whereas in the 3 drug-treated groups, an equal dose of 30 mg/kg/administration was orally administered twice daily for 3 weeks, that is, a daily dose of 60 mg/kg in each group. Body weight and food intake were recorded per week. At the end of the experiment, after fasting for 14 h, all mice were anesthetized with amobarbital sodium (45 mg/kg) via intraperitoneal injection and euthanized. Serum was obtained, and liver tissue was removed immediately and weighed to calculate the hepatic index (percentage of body weight). A section of liver tissue from each mouse was fixed immediately in 10% neutral buffered formalin, and the remaining liver tissue and serum samples were stored at -80°C until further processing and analysis.

HepG2 cell culture and PMH isolation and culture

The human hepatocarcinoma (HepG2) cell line, purchased from the Stem Cell Bank, Chinese Academy of Sciences (Shanghai, China), was cultured in DMEM supplemented with 10% FBS and 1% penicillin/streptomycin and maintained at 37°C in a 5% CO_2 atmosphere. When treated, the cells were incubated with serum-free (to exclude the influence of serum 5-HT on the results) and antibiotics-containing DMEM. After incubation for 1 h, the cells were treated with drug or an equal-volume of phosphate-buffered saline (PBS) for 30 min, then additionally exposed to vehicle (50% isopropanol for PA, PBS for 5-HT), PA, or 5-HT, respectively, according to each experiment.

C57BL/6J mice (6–8 weeks old), purchased from the Comparative Medicine Center of Yangzhou University (Jiangsu, China), were anesthetized with amobarbital sodium, and PMHs were obtained via a two-step perfusion method as described previously [18]. Then, PMH suspensions were filtered through a 100-μm cell strainer and centrifuged at 100 × *g* for 2 min. The cell pellet containing PMHs was resuspended in Williams E medium supplemented with 10% FBS and 1% penicillin/streptomycin and cultured. At 8 h after plating, unattached cells were removed by washing, and fresh medium was added and the cells were incubated further for 24 h. Then, the cells were incubated with serum-free Williams E medium and treated with drug or equal-volume PBS for 30 min, and additionally exposed to vehicle (50% isopropanol for PA, PBS for D-glucose), PA, or D-glucose, respectively, according to each experiment.

Small interfering RNA by using lentiviral infections or plasmid transfections

As in a previous study [12], we silenced the expression of Tph1 (siTph1), 5-HT_{2A}R (si5-HT_{2A}R), 5-HT_{2B}R (si5-HT_{2B}R), and Gαq (siGαq) using a recombinant lentivirus. Target short hairpin RNAs (shRNAs) against human Tph1, 5-HT_{2A}R, 5-HT_{2B}R, and Gαq genes for RNA interference were designed and synthesized by GenePharma (Shanghai, China) as follows: Tph1 (5′-CGG GAG GAT AAT ATC CCA CAA-3′), 5-HT_{2A}R (5′-CCC TGC TCA ATG TGT TTG TTT-3′), 5-HT_{2B}R (5′-CCG ATA TAT CAC CTG CAA TTA-3′), Gαq (5′-GCA AGA GTA CGT TTA TCA AGC-3′), and the lentiviral vector GV248-negative (shRNA control) (siCtrl): 5′-TTC TCC GAA CGT GTC ACG T-3′ without suppression of the expression of human genes. Polybrene was added to the lentivirus supernatant until a final concentration of 5 μg/mL. The supernatant was used to infect HepG2 cells for 12 h and then placed in fresh medium for another 72 h. After infection, the fluorescence of green fluorescent protein (GFP) was detected using a fluorescence inversion microscope system (Monolith; Olympus, Tokyo, Japan). Infected HepG2 cells were seeded into DMEM supplemented with 10% FBS in an appropriate plate or culture flask and incubated according to requirement, and were then incubated in serum-free medium with or without drug or/and PA treatment, as for HepG2 cell culture.

We silenced the expression of MAO-A (siMAO-A) and NF-κB p65 (siNF-κB p65) using the recombinant plasmid pGPU6/GFP/Neo with shRNA against MAO-A (5′-GGA TAT TCT CTG TCA CCA ATG-3′), NF-κB p65 (5′-GCC AGA TAC AGA CGA TCG TCA-3′), and negative control (siCtrl) (5′-TTC TCC GAA CGT GTC ACG T-3′) designed and synthesized by GenePharma. The plasmid with siMAO-A, siNF-κB p65, or siCtrl was used to transfect HepG2 cells with Entanster™-H4000 reagent according to the manufacturer's specifications. Briefly, the cells were incubated with DMEM containing 10% FBS for approximately 24 h. When cell density reached 60%, the target plasmid and Entanster™-H4000 were added and incubated with fresh DMEM and FBS for 48 h. After transfection, GFP fluorescence was detected via a fluorescence inversion microscope system (Monolith; Olympus, Tokyo, Japan). When the cells were used in the experiments, they were incubated with serum-free DMEM.

Measurement of ROS generation and localization of mitochondria

Detection of ROS levels or co-localization of intracellular ROS and mitochondria were performed using the fluorescent dye DCFH-DA or the combination of DCFH-DA and MitoTracker® Red CMXRos (mitochondria-specific probe), respectively. HepG2 cells (1.0×10^6 cells/mL) were incubated in a laser confocal culture dish with MitoTracker® Red CMXRos and/or DCFH-DA for 30 min in the dark at 37°C. After washing 3 times with PBS, HepG2 cells were examined under a confocal laser scanning microscope (LSM700; Zeiss, Oberkochen, Germany). The excitation wavelengths for DCFH-DA and MitoTracker® Red CMXRos are 488 and 579 nm, respectively, to detect ROS levels and ROS and mitochondria localization.

Western blot analysis

Extraction of whole cell, plasmalemma, cytosol, and nucleoplasm proteins was performed using protein extraction kits, respectively. Protein concentration was determined by an Enhanced BCA Protein Assay Kit to calculate the loading amount. Samples were separated by SDS-PAGE and electrophoretically transferred to a polyvinylidene fluoride membrane. Nonspecific binding sites were blocked with Tris-buffered saline containing 5% bovine serum albumin for 2 h at a room temperature. After being washed with TBST, the membranes were incubated with specific primary antibodies at 4°C overnight, respectively. Then, the membranes were incubated with horseradish peroxidase-coupled secondary antibodies. Immunopositive bands were visualized by a chemiluminescent method (ECL, Tanon-5200, China), and the protein bands were quantified by densitometry. Parallel blotting of β-actin for cytosol or whole-cell proteins, Na^+-K^+-ATPase for plasmalemma proteins, and lamin-B1 for nucleoplasm proteins was used as an internal control.

Reverse transcription polymerase chain reaction analysis

Total RNA was isolated from cells using RNAiso plus Isolation Reagent (TAKARA, Shiga, Japan). Total RNA was first reverse transcribed and then immediately amplified in a GeneAmp PCR system (Eppendorf). The following primers were used: NF-κB p65 (forward-CAT CCA GAC CAA CAA CAA C; reverse-TCC TTT TAC TTT CTC CTC A), IL-1β (forward-CCA GTG AAA TGA TGG CTT AT; reverse-TGT AGA GTG GGC TTA TCA TC), TNF-α (forward-ACT TTA AGC AAC AAG ACC AC; reverse-TAT TGT TCA GCT CCG TTT TC), IL-6 (forward-GGA GAG GGA GCG ATA AAC; reverse-TGG ATC AGG ACT TTT GTA CT), and GAPDH (forward-TGA CTA ACC CTG CGC TC; reverse-ATG AGT CCT TCC ACG ATA C). The gel was photographed by a Gel Image System (ECL, Tanon-3500, China) and the bands on the film were scanned by densitometry for quantitation. To exclude variations due to RNA quantity and quality, the data for all genes were adjusted to the expression of GAPDH.

Oil red O, hematoxylin and eosin, and Masson's trichrome staining

HepG2 cells or PMHs were fixed with 4% paraformaldehyde, rinsed with 60% isopropanol or PBS, respectively, and stained with freshly prepared Oil red O working solution and rinsed with 60% isopropanol or PBS again; finally, they were counterstained with hematoxylin. The cells were examined under an optical microscope (Monolith; Olympus, Tokyo, Japan).

For histopathological examinations, formalin-fixed liver tissue was sectioned and processed routinely for hematoxylin and eosin or Masson's trichrome staining. Histopathological examinations were performed by a trained pathologist using an optical microscope (Monolith; Olympus, Tokyo, Japan). Hepatic steatosis, inflammation, and fibrosis of each liver sample were assessed.

Detecting indicators with ELISA kits or enzyme-test kits

Insulin, VLDL, L-dopamine, 5-HT, TNF-α, IL-1β, IL-6, DAG, IP3, and hydroxyproline levels in the serum, liver tissue, medium, or cultured cells were assessed in a microplate using respective commercial ELISA kits with a microplate reader (infinite M200PRO; TECAN, Männedorf, Switzerland). The concentration of the indicators was calculated according to a standard curve. The indicators in liver tissue, medium, or cells were divided by the corresponding protein concentration to obtain the final results.

AST, ALT, glucose, TG (only in serum), FFAs, LDL-c, H_2O_2, MDA, and HDL-c levels in the serum, liver tissue, or cells were assessed using respective commercial assay kits with a microplate reader (infinite M200PRO; TECAN, Männedorf, Switzerland). The concentration of the indicators was calculated according to a standard curve. VLDL-c was calculated by TC – (LDL-c + HDL-c). The Homeostasis Model of Assessment–IR (HOMA-IR) index, a measure of IR, was calculated as serum glucose × serum insulin/22.5.

TG analysis in cells and liver tissue

Liver tissue and cell samples were heated at 70°C for 10 min and centrifuged at 600 × *g* for 5 min. The supernatant was used to determine the content of TG in liver tissue and cells. According to the TG enzyme-test kit instructions, the absorbance values were measured at a wavelength of 550 nm with a microplate reader (infinite M200PRO; TECAN). The concentration of TG was calculated according to a standard curve. TG concentration in liver tissue and cell samples was divided by the corresponding protein concentration to obtain the final results.

Statistical analysis

Data are expressed as the mean ± standard deviation (SD). Differences between the groups were tested for statistical significance using one-way analysis of variance followed by the least significant difference multiple comparison test, while differences in the expression levels of hepatic Tph1, AADC, 5-HT_{2A}R, and 5-HT_{2B}R between two groups were tested using Student's t-test. *P*-values < 0.05 were considered significant.

Results

PA-induced ELS and PICG with 5-HT system activation in HepG2 cells

PKCε is a key PKC for the exacerbation of SFA-induced lipogenesis with IR in hepatocytes [2]. DAG, via its binding to PKCε, promotes the translocation of PKCε from the cytoplasm to the cytomembrane with PKCε activation [19]. NF-κB is one of the most important transcription factors for the initiation of pro-inflammatory gene transcription and it is activated in NASH [20], implicating it in the etiology of IR [21]. In the quiescent state, IκB binds to NF-κB to prevent its activation. When IκB is ubiquitinated and degraded, NF-κB is released and translocates into the nucleus, which initiates the transcription of pro-inflammatory genes (e.g., TNF-α and IL-1β) with PICG [22]. In this study, we detected PICG mainly through the measurement of TNF-α and IL-1β levels in cells.

A high level of blood FFAs is a key factor in the pathogenesis of NAFLD and IR [23]. To clarify the relationship between ELS, PICG, and 5-HT system activation in FA-treated hepatocytes, HepG2 cells were exposed to PA *in vitro*. Initially, the cells were treated with PA at different time points. We found that the activation of the 5-HT system,

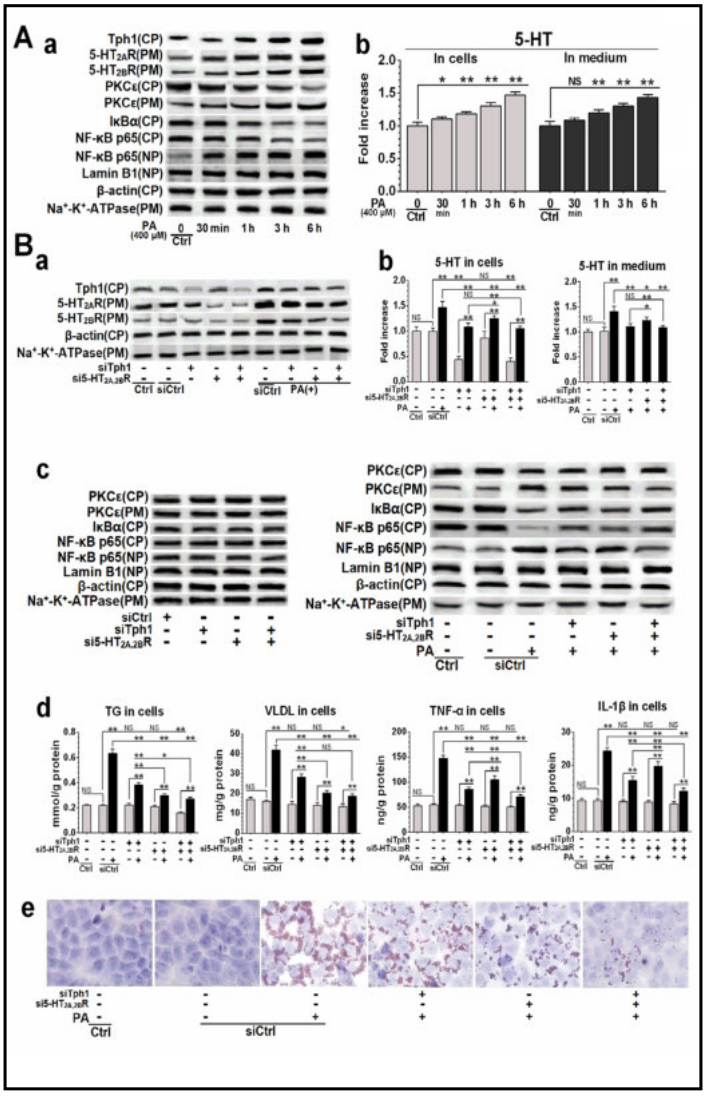

Fig. 1. Time-dependent effects of PA on the activation of the 5-HT system, PKCε, and NF-κB in HepG2 cells, and the effects of genetic inhibition of Tph1 and 5-HT_2R (alone or in combination) on PA action. A: Cells were treated with 400 μM PA for 0–6 h, and protein levels (a) and 5-HT levels (b) were examined. B: Except for Ctrl cells, cells with siCtrl, siTph1, and si5-$HT_{2A,2B}$R (alone or in combination) were incubated with or without 400 μM PA for 3 h (a–c) or 24 h (d, e). Protein levels (a) of components of the 5-HT system and 5-HT levels (b), protein levels of PKCε, IκBα, and NF-κB p65 (c), levels of TG, VLDL, TNF-α, and IL-1β (d), and lipid droplets determined by Oil red O staining (40×) (e). Data are presented as the mean ± SD of 3 independent experiments. *P<0.05; **P<0.01. Abbreviations: NS, not significant; CP, cytoplasm; PM, plasmalemma; NP, nucleoplasm.

PKCε, and NF-κB was time-dependent and synchronous within 6 h after PA treatment, including increased 5-HT_{2A}R, 5-HT_{2B}R, and Tph1 expression with increased intracellular and extracellular 5-HT levels, increased PKCε expression in the plasmalemma but decreased PKCε expression in the cytoplasm, decreased IκBα and NF-κB p65 expression in the cytoplasm, and increased NF-κB p65 expression in the nucleoplasm (Fig. 1A). At 3 h after PA treatment, the above changes were observed clearly.

Next, to identify the role of the 5-HT system in the action of PA in hepatocytes, we suppressed Tph1, 5-HT_{2A}R, and 5-HT_{2B}R expression using a gene-silencing method. Gene-silencing control (siCtrl), using negative lentiviral vector treatment, did not affect cell phenotype (Fig. 1B, a–e) as compared with the control cells. Compared with siCtrl cells, silencing Tph1 (siTph1), or silencing both 5-HT_{2A}R and 5-HT_{2B}R (si5-$HT_{2A,2B}$R), strongly reduced their expression levels by approximately 70% (Fig. 1B, a). In addition, siTph1 or si5-$HT_{2A,2B}$R greatly suppressed the PA-induced upregulation of their respective expression (Fig. 1B, a), and siTph1 reduced intracellular and culture medium 5-HT levels in normal and PA-treated cells; si5-$HT_{2A,2B}$R also suppressed the PA-induced increases in Tph1 expression and intracellular and extracellular 5-HT levels (Fig. 1B, a and b), whereas both hardly affected the phenotype of normal cultured cells, including PKCε, NF-κB activity, and intracellular levels of TG, VLDL, TNF-α, and IL-1β (Fig. 1B, c [left] and d). SiTph1 and si5-$HT_{2A,2B}$R (alone or in combination) showed different effects on PA action, for which the inhibitory effects of siTph1 on PA-induced NF-κB activation (Fig. 1B, c [right]) and PICG with increased levels of intracellular TNF-α and IL-1β (Fig. 1B, d) were greater than with si5-$HT_{2A,2B}$R, while for PA-induced PKCε activation (Fig. 1B, c [right]) and ELS with increased levels of intracellular TG and VLDL with LDA (Fig. 1B, d and e), si5-$HT_{2A,2B}$R was stronger than siTph1. A combination of siTph1 and si5-$HT_{2A,2B}$R strongly suppressed PA-induced cellular dysfunction (Fig. 1B, c–e) with a synergistic inhibitory effect between both, suggesting that the activation of the 5-HT system is required for PA-induced dysfunction in ELS and PICG in HepG2 cells.

Source of DAG that activates PKCε in PA-treated HepG2 cells

Hepatocellular DAG can be produced via two pathways: from TG synthesis in lipid droplets [24]; and as a consequence of the activation of G protein-coupled receptors, such as 5-HT_{2A}R and 5-HT_{2B}R with G protein $G_{q/11}$ activation, primarily G_q [25], in the cytomembrane, leading to the activation of phospholipase C (PLC)-catalyzed hydrolysis of phosphatidylinositol bisphosphate and the production of both DAG and IP3.

To examine if G_q has a key role in PA- and 5-HT-induced PKCε activation, we gene-silenced $G\alpha_q$ (si$G\alpha_q$). SiCtrl did not affect $G\alpha_q$ expression as compared with Ctrl cells (Fig. 2A, a [up]), while si$G\alpha_q$ reduced $G\alpha_q$ expression by approximately 80% as compared with siCtrl cells, and also strongly reduced the PA- and 5-HT-induced upregulation of $G\alpha_q$ expression (Fig. 2A, a). By examining the expression of PKCε in the plasmalemma (Fig. 2A, a) and the intracellular levels of DAG and IP3 (Fig. 2A, b), si$G\alpha_q$ was found to suppress strongly the PA- and 5-HT-induced enhancement of intracellular DAG and IP3 levels with PKCε activation, suggesting that $G\alpha_q$ activation mediates PA- and 5-HT-induced PKCε activation in these cells.

Next, we examined the relationship between PKCε activation and PLC activity to ascertain the origin of DAG causing PKCε activation. We employed the PLC antagonist U-73122 [26] to inhibit PLC activity, and triacsin C [27] was used to inhibit acyl-CoA synthase activity. Acyl-CoA synthase transforms FFAs to their long-chain fatty acyl-coenzyme A derivatives to control TG synthesis in lipid droplets, β-oxidation in mitochondria, and the synthesis of membrane phospholipids [28]; therefore, triacsin C can inhibit acyl-CoA synthase-mediated lipid droplet TG synthesis with DAG generation. In parallel with suppressing the PA-induced upregulation of 5-$HT_{2A,2B}$R expression (Fig. 2B, a), si5-$HT_{2A,2B}$R also strongly suppressed the PA-induced upregulation of $G\alpha_q$ expression, whereas upregulated $G\alpha_q$ was not suppressed by U-73122 (Fig. 2B, b), indicating that PA-induced G_q activation is due to the activation of 5-HT_2R. We also found (Fig. 2B, c and d): (1) both si5-$HT_{2A,2B}$R and U-73122 treatment had similar inhibitory effects on PA-induced PKCε activation, up-regulation of GPAT1 (a rate-limiting enzyme of TG synthesis) expression, and increased the intracellular levels of

DAG, IP3, and TG. Additionally, U-73122 treatment showed slight inhibitory effects in the siCtrl cells; (2) triacsin C treatment merely showed inhibitory effects on the PA-induced upregulation of GPAT1 expression and increases in DAG and TG levels, but did not affect PKCε activation or increase IP3 levels; and (3) the alteration of PKCε levels in the cytomembrane was in accordance with the alteration of IP3 levels in all groups, suggesting that the origin of DAG that activates PKCε is associated with IP3, and not from TG synthesis.

Taken together, activated 5-HT$_2$R mediates G$_q$ activation, leading to increased PLC activity with DAG and IP3 generation in the cytomembrane, ultimately resulting in PKCε activation in PA-treated cells.

5-HT$_2$R causes PKCε activation with ELS and PICG in PA-treated HepG2 cells

PKCε activation has been demonstrated to result in IR [2, 29]. Activated PKCε mediates the phosphorylation of both Akt, which further regulates the phosphorylation of mTOR, and ERK, thereby modulating cellular survival, metabolism, and so on [30]. In the regulation of lipid anabolism, ACC is a rate-limiting enzyme of *de novo* lipogenesis, GPAT1 limits the rate of TG synthesis, while the rate of VLDL assembly is limited by MTTP [5].

To examine 5-HT$_2$R-mediated PKCε activation and PKCε-controlled downstream molecules, and to clarify the effects of the 5-HT$_2$R/PKCε pathway on ELS and PICG, we employed PIP to inhibit PKCε [31], while saponin (which did not affect cell phenotype) was used to transport PIP across the cytomembrane in HepG2 cells. We also employed both siTph1 and si5-HT$_{2A,2B}$R (siTph1+si5-HT$_{2A,2B}$R) to suppress 5-HT$_2$R activity fully. In this experiment, PA-induced PKCε activation with upregulated PKCε expression in the cytomembrane was completely suppressed by PIP and also strongly suppressed by siTph1+si5-HT$_{2A,2B}$R (Fig.

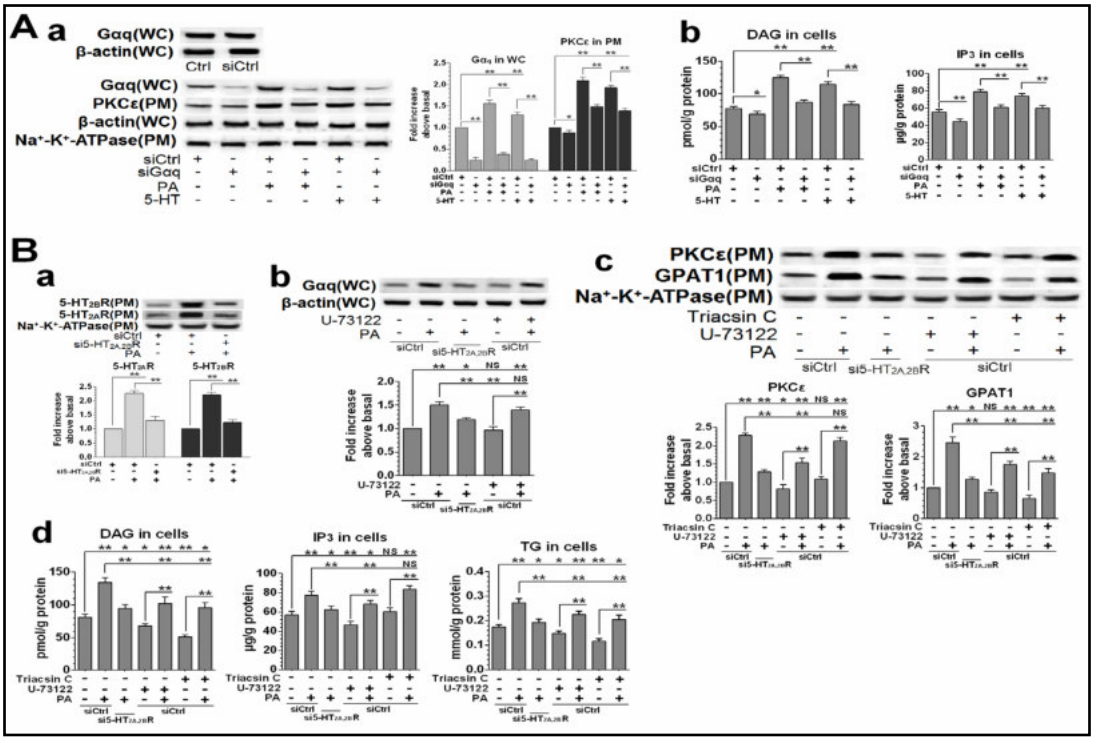

Fig. 2. 5-HT$_2$R mediates PKCε activation through G$_q$ activation in PA-treated HepG2 cells. A: Except for Ctrl cells, siCtrl and siGα$_q$ cells were treated with or without either PA (400 μM) or 5-HT (50 μM) for 6 h; protein levels and densitometric analysis (a), and DAG and IP3 levels (b). B: siCtrl cells were treated with or without triacsin C (7.5 μM) or U-73122 (15 μM) and treated with or without PA (400 μM), and si5-HT$_{2A,2B}$R cells were treated with PA for 6 h. Protein levels and densitometric analysis (a–c); DAG, IP3, and TG levels (d). Data are presented as the mean ± SD of 3 independent experiments. *P<0.05; **P<0.01. Abbreviations: NS, not significant; IP3, inositol triphosphate; WC, whole cells; PM, plasmalemma.

3a). Whereas PIP did not affect the PA-induced activation of the 5-HT system, including the upregulation of Tph1, 5-HT_{2A}R, and 5-HT_{2B}R expression (Fig. 3a), and increased 5-HT levels (Fig. 3b), indicating there is no feedback between PKCε and the 5-HT system. Significant inhibitory effects of both siTph1+si5-$HT_{2A,2B}$R and PIP were observed on the PA-induced phosphorylation of Akt, mTOR, and ERK1/2 (Fig. 3a) and ELS with the upregulation of ACC, GPAT1, and MTTP expression (Fig. 3c) and increased levels of TG and VLDL with LDA (Fig. 3d and e), while the inhibitory effects of siTph1+si5-$HT_{2A,2B}$R were greater than those of PIP, suggesting that PKCε activation is a pivotal, but not unique, pathway for PA-induced and 5-HT system-modulated ELS in cells. For PA-induced PICG, the inhibitory effects of PIP were far less than those of siTph1+si5-$HT_{2A,2B}$R, for which the inhibitory extent of PIP on PA-induced NF-κB activation (Fig. 3c) and generation of TNF-α and IL-1β (Fig. 3d) were far less than that of siTph1+si5-$HT_{2A,2B}$R, indicating that PKCε activation is not key for PA-induced and 5-HT system-modulated PICG in cells.

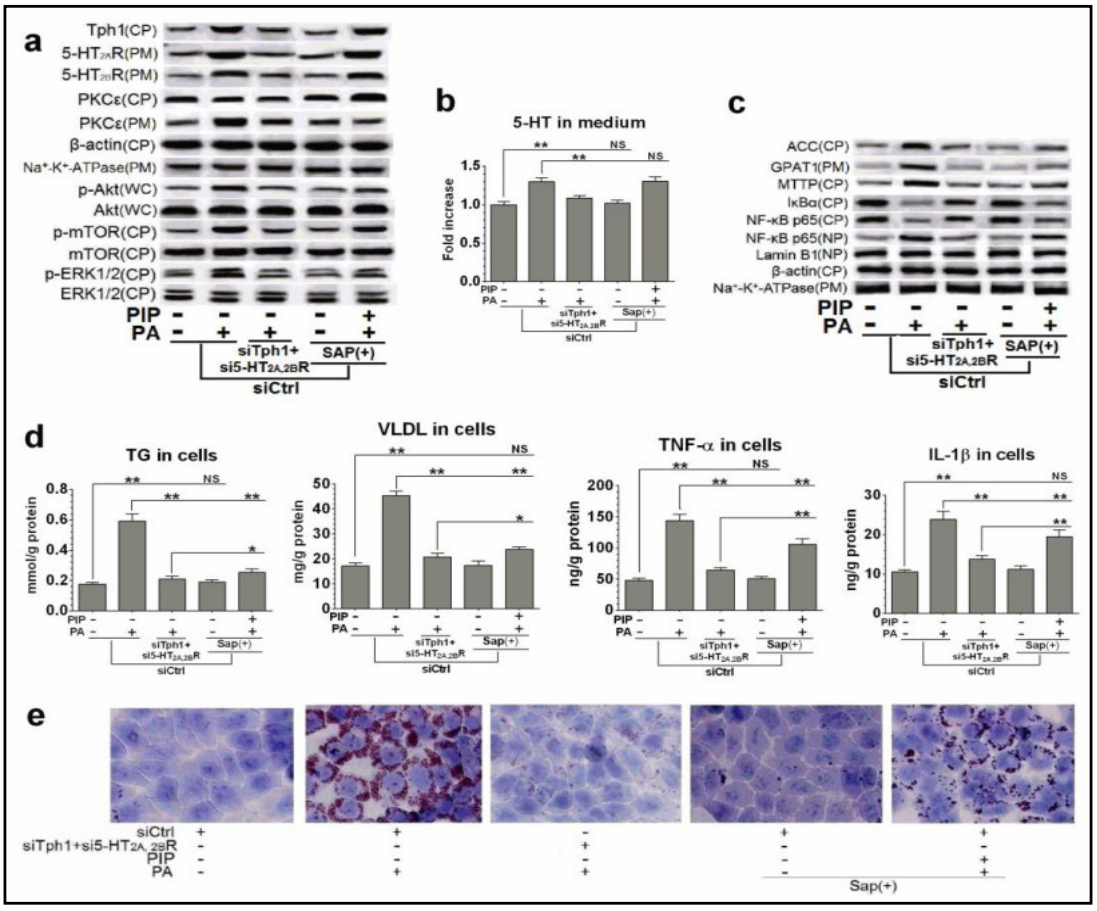

Fig. 3. Relationship between 5-HT_2R-mediated PKCε activation and ELS and PICG in PA-treated HepG2 cells. siCtrl cells were treated with or without PA (400 μM), with Sap (50 μg/mL), or with Sap, PIP (15 μM), and PA, or siTph1+si5-$HT_{2A,2B}$R cells were treated with PA for 3 h (a, b) or 24 h (c–e). Protein levels (a, c) and 5-HT levels (b), TG, VLDL, TNF-α, and IL-1β levels (d), and lipid droplets determined by Oil red O staining (40×) (e). Data are presented as the mean ± SD of 3 independent experiments. *P<0.05; **P<0.01. Abbreviations: NS, not significant; Sap, saponin; PIP, PKC inhibitor peptide; CP, cytoplasm; PM, plasmalemma; NP, nucleoplasm; p-, phosphorylated; WC, whole cells.

Effects of 5-HT$_{2A}$R and 5-HT$_{2B}$R activated by 5-HT

To clarify the functions of 5-HT$_{2A}$R and 5-HT$_{2B}$R in the activation of PKCε with ELS, we silenced the expression of 5-HT$_{2A}$R and 5-HT$_{2B}$R (alone or in combination) in 5-HT-treated HepG2 cells. Si5-HT$_{2A}$R and si5-HT$_{2B}$R showed a similar inhibitory effect, respectively, on the 5-HT-induced upregulation of 5-HT$_{2A}$R and 5-HT$_{2B}$R expression (Fig. 4A, a), whereas their effect on 5-HT-induced ELS was distinguishable. 5-HT caused the activation of PKCε (Fig. 4A, a) and upregulated GPAT1 and MTTP expression (Fig. 4A, a), and the increases in intracellular TG and VLDL (Fig. 4A, b) were strongly suppressed by si5-HT$_{2A}$R+si5-HT$_{2B}$R, whereas the

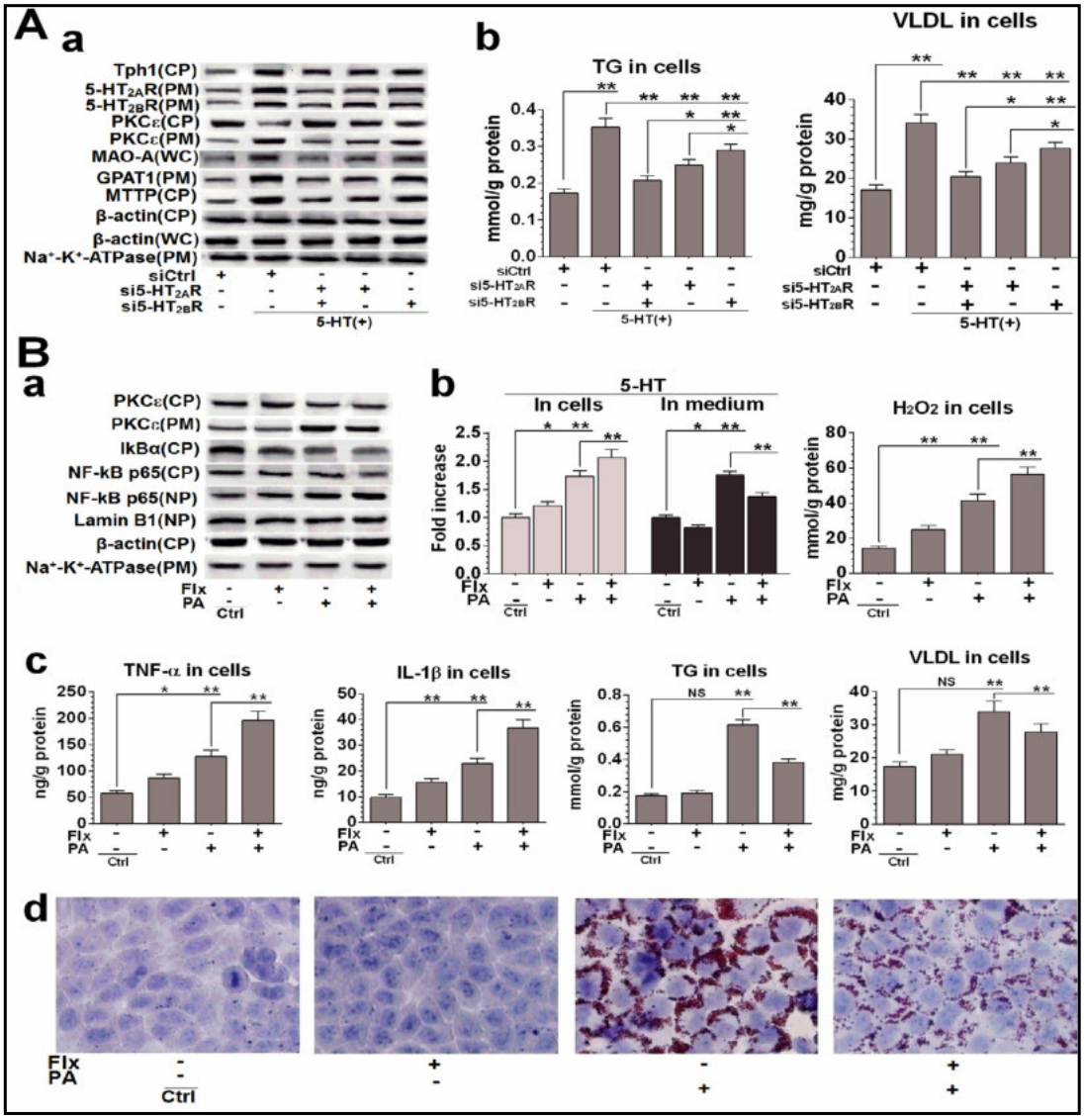

Fig. 4. Effects of 5-HT$_{2A}$R and 5-HT$_{2B}$R and effects of intracellular 5-HT in PA-treated HepG2 cells. A: siCtrl cells were treated with or without 5-HT (100 μM), or si5-HT$_{2A}$R and si5-HT$_{2B}$R (alone or in combination) cells were treated with 5-HT for 3 h (a) or 24 h (b). Protein levels (a) and TG and VLDL levels (b). B: Normal or Flx (50 μM)-treated HepG2 cells were treated with or without PA (400 μM) for 3 h (a) or 24 h (b–d). Protein levels (a), 5-HT and H_2O_2 levels (b), TNF-α, IL-1β, TG, and VLDL levels (c), and lipid droplets determined by Oil red O staining (40×) (d). Data are presented as the mean ± SD of 3 independent experiments. *P<0.05; **P<0.01. Abbreviations: NS, not significant; Flx, fluoxetine; CP, cytoplasm; PM, plasmalemma; NP, nucleoplasm; WC, whole cells.

individual effects of si5-HT_{2A}R and si5-HT_{2B}R were less than those of their combination; the effects of si5-HT_{2A}R were also stronger than those of si5-HT_{2B}R. In addition, si5-HT_{2A}R and si5-HT_{2B}R showed inhibitory effects on the 5-HT-induced upregulation of Tph1 and MAO-A expression (Fig. 4A, a), primarily by si5-HT_{2A}R. These data indicate that the activation of 5-HT_{2A}R plays a primary role in mediating PKCε activation with ELS, and also mediates the upregulation of 5-HT synthesis and MAO-A expression.

5-HT degradation with PICG in PA-treated HepG2 cells

To clarify if another 5-HT-mediated pathway affected PICG and PKCε in PA-treated HepG2 cells, we used Flx, a blocker of 5-HT transporters, to inhibit 5-HT output from cells. Flx treatment increased the intracellular levels of 5-HT, but decreased its extracellular levels, in both PA-treated and normal cells (Fig. 4B, b). Correspondingly, Flx exacerbated PA-induced PICG with increased intracellular levels of H_2O_2, TNF-α, and IL-1β and the activation of NF-κB; these effects were also found in normal cells, but to a lesser extent (Fig. 4B, a–c). Conversely, Flx reversed PA-induced ELS with PKCε activation and increased the intracellular levels of TG and VLDL with LDA, whereas this effect was not found in normal cells (Fig. 4B, a, c, and d). These data suggested that the intracellular level of 5-HT is related to PICG, while its extracellular level is related to ELS in PA-treated HepG2 cells.

Next, we clarified how intracellular 5-HT leads to PICG in PA-treated HepG2 cells. We hypothesized that the effect of intracellular 5-HT on promoting PICG could be attributed to its degradation by MAO-A in the mitochondria, thereby generating ROS, mainly H_2O_2 [7]. Indeed, the intensity of PICG was in accordance with the levels of intracellular 5-HT and H_2O_2 (Fig. 4B, b). To confirm this observation, we employed CGN and Sar to inhibit MAO-A and 5-HT_2R activity, respectively. To observe the intracellular distribution of ROS, we employed the fluorescent probe DCFH-DA to detect intracellular ROS levels and MitoTracker® Red CMXRos to localize the mitochondria. In PA-treated cells, CGN further increased 5-HT levels, while Sar reversed this increase (Fig. 5A, b). CGN and Sar significantly reversed PA-induced NF-κB activation with increased intracellular levels of H_2O_2 and TNF-α in a synergistic inhibitory manner (Fig. 5A, a, b, and d). By fluorescent dye staining, we observed that ROS and mitochondria co-localized in PA-treated cells (Fig. 5A, c), and that the amount of ROS in each group was in accordance with H_2O_2 levels; this PA-induced production of ROS and H_2O_2 was inhibited by CGN and Sar (alone or in combination) in a synergistic manner (Fig. 5A, d), suggesting that the PA-induced production of ROS originates from mitochondria, releasing them into the cytoplasm, and that these ROS with H_2O_2 are crucially dependent on MAO-A-catalyzed 5-HT degradation in the mitochondria. Additionally, the PA-induced increase in intracellular TG levels with LDA was exacerbated by CGN, but was attenuated by Sar (Fig. 5A, d), again indicating that TG synthesis is dependent on the action of extracellular 5-HT on 5-HT_2R when the cells are exposed to PA.

To further confirm the relationship between 5-HT degradation and PICG in PA-treated cells, we silenced MAO-A expression (siMAO-A) using a plasmid vector to suppress MAO-A activity. MAO-A expression was strongly reduced by siMAO-A in normal HepG2 cells (Fig. 5B, a) and was markedly upregulated by PA, while the increased expression of MAO-A by PA was markedly suppressed by siMAO-A or the combination of siMAO-A and Sar (Fig. 5B, a). The effects of siMAO-A with or without Sar treatment were very similar to those of CGN with or without Sar treatment on PA-induced NF-κB activation and increased the cellular levels of 5-HT, H_2O_2, and TNF-α (Fig. 5B, a and b). More importantly, PA-induced PICG was almost completely inhibited by the combination of siMAO-A and Sar, suggesting that PICG in PA-treated hepatocytes is attributed to the increased degradation of 5-HT by MAO-A and 5-HT_2R activity.

To confirm that PICG in PA-treated cells is controlled by NF-κB, we silenced NF-κB p65 expression (siNF-κB p65) using a plasmid vector to suppress NF-κB activity, and made a comparison between siNF-κB p65 and co-treatment with pCPA and Sar (inhibitor of Tph1 and 5-HT_2R, respectively, to inhibit the 5-HT system). The expression levels of NF-κB p65 messenger RNA (mRNA) and protein in normal and PA-treated cells were strongly reduced

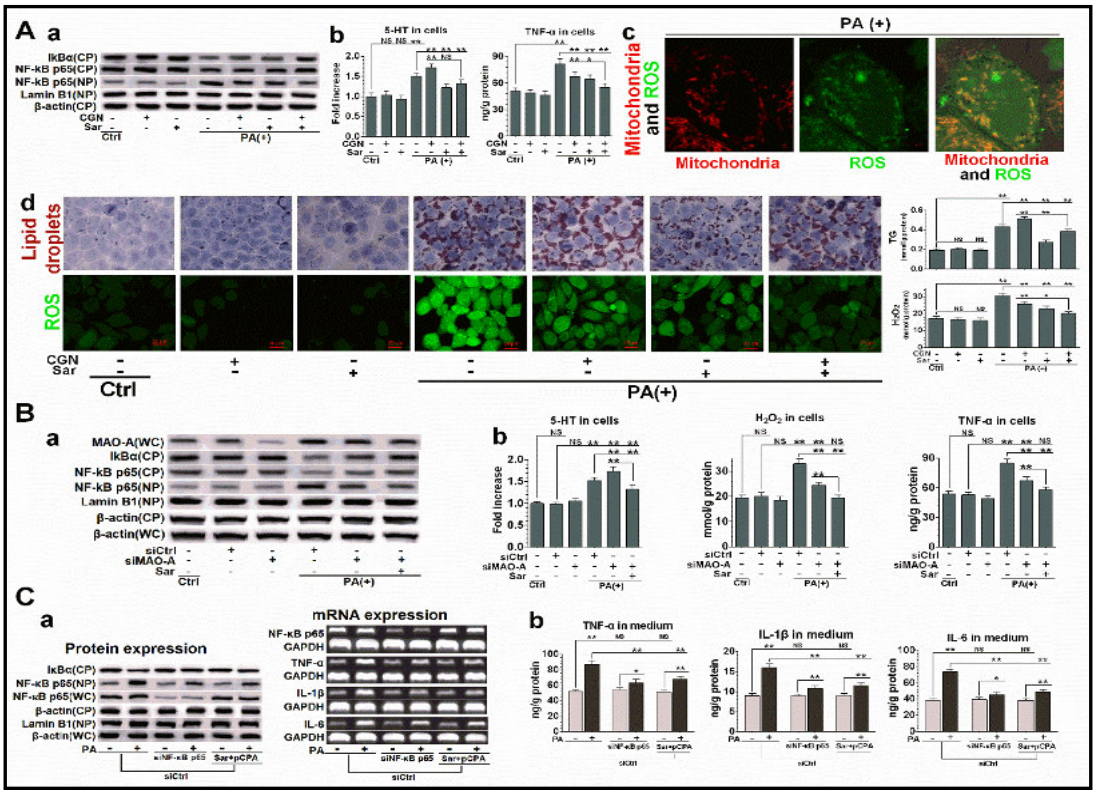

Fig. 5. Relationship between 5-HT degradation and PICG in PA-treated HepG2 cells. A: Normal, CGN (10 μM)-, or Sar (50 μM)-treated cells were treated with or without PA (200 μM); CGN+Sar-treated cells were treated with PA for 24 h. Protein levels (a), 5-HT and TNF-α levels in the cells (b), mitochondria location and ROS distribution in PA-treated cells determined by fluorescent dye staining (63×) (c), and lipid droplets determined by Oil red O staining (40×) and TG levels, ROS distribution (20×), and H_2O_2 levels in the cells (d). B: Except for Ctrl, siCtrl and siMAO-A cells were treated with or without PA (200 μM), and siMAO-A cells were treated with both Sar (50 μM) and PA for 24 h. Protein levels (a) and 5-HT, H_2O_2, and TNF-α levels (b). C: siCtrl, siNF-κB p65, and co-treated with pCPA (50 μM) and Sar (50 μM) cells were treated with or without PA (400 μM) for 12 h. Protein and mRNA levels (a) and culture medium levels of TNF-α, IL-1β, and IL-6 (b). Data are presented as the mean ± SD of 3 independent experiments. $^{*}P<0.05$, $^{**}P<0.01$. Abbreviations: NS, not significant; pCPA, para-chlorophenylalanine; Sar, sarpogrelate; CGN, clorgiline; CP, cytoplasm; NP, nucleoplasm; WC, whole cells.

by siNF-κB p65, but were not affected by PA or co-treatment with pCPA and Sar (Fig. 5C, a), while siNF-κB p65 and co-treatment with pCPA and Sar showed similar inhibitory effects on PA-induced NF-κB activation, upregulation of TNF-α, IL-1β, and IL-6 mRNA, and increased the levels of these cytokines in culture medium (Fig. 5C, a and b), suggesting that PA-induced PICG in HepG2 cells is through the NF-κB-controlled increase of the mRNA levels of pro-inflammatory cytokines, which is mediated by the 5-HT system.

Taken together, in PA-treated HepG2 cells, ROS levels (primarily H_2O_2) were increased in the mitochondria as the key factor for PA-induced PICG, as a result of MAO-A-catalyzed 5-HT degradation, leading to NF-κB activation and the NF-κB-controlled increase in the mRNA expression of pro-inflammatory cytokines, ultimately resulting in the increased synthesis and secretion of these cytokines.

PA-induced 5-HT system activation, ELS, and PICG in PMHs

In this experiment, we detected the phosphorylation of three MAP kinases (p38, JNK, and ERK1/2) and STAT3 in addition to the aforementioned factors, all of which are involved in inflammation and IR [32]. The expression of the 5-HT system and 5-HT levels were also up-

regulated by PA in PMHs (Fig. 6A, a), and PA-induced ELS and PICG, including activated PKCε and NF-κB, increased the phosphorylation of p38, JNK, ERK1/2, STAT3, Akt, and mTOR (Fig. 6A, b), increased the intracellular levels of TG with LDA, VLDL, H_2O_2, and MDA (indicating oxidative stress) (Fig. 6A, c and e), and increased intracellular and extracellular levels of TNF-α, IL-1β, and IL-6 (Fig. 6A, d), which were strongly suppressed by pCPA + Sar, whereas these drugs had no effect in normal PMHs.

We conclude that besides modulating PKCε activation with subsequent ELS, the SFA-induced activation of the 5-HT system also modulates complicated inflammatory processes by controlling multiple inflammatory signaling pathways and NF-κB activation, leading to the increased biosynthesis and release of multiple pro-inflammatory cytokines by hepatocytes.

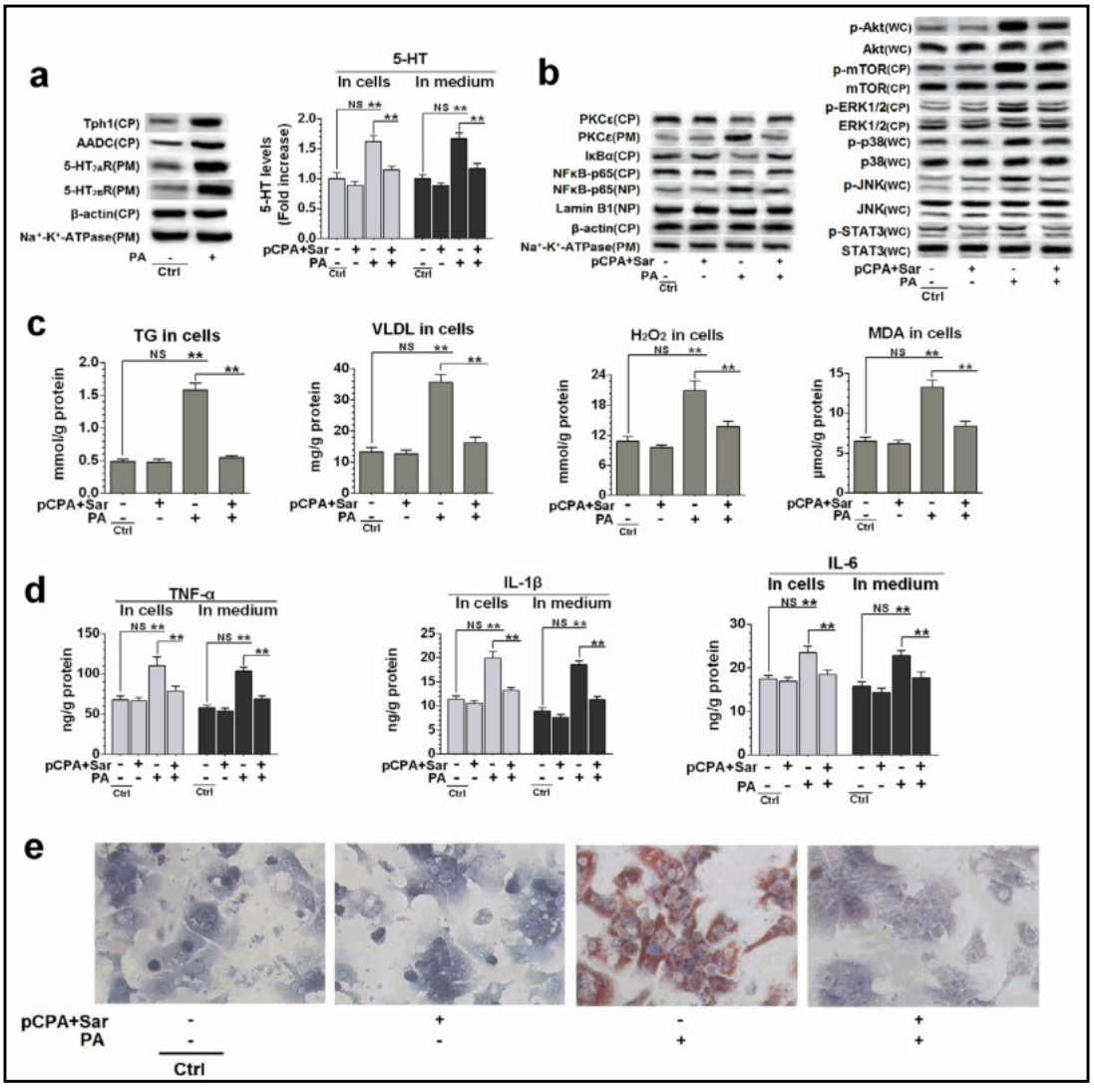

Fig. 6. Relationship between 5-HT system activation and PA-induced ELS and PICG in PMHs. Normal cells and cells co-treated with pCPA (30 μM) and Sar (30 μM) were treated with or without PA (400 μM) for 3 h (a, b) or 10 h (c–e). (a, b) Protein levels and 5-HT levels. (c, d) Levels of TG, VLDL, H_2O_2, MDA, TNF-α, IL-1β, and IL-6. (e) Lipid droplets determined by Oil red O staining (40×). Data are presented as the mean ± SD of 3 independent experiments. $^{*}P<0.05$, $^{**}P<0.01$. Abbreviations: NS, not significant; Sar, sarpogrelate; pCPA, para-chlorophenylalanine; CP, cytoplasm; PM, plasmalemma; NP, nucleoplasm; WC, whole cells; p-, phosphorylated.

HG-induced 5-HT system activation, TG overproduction, and PICG in PMHs

HG may be another factor leading to the development of NASH. In the HFD+STZ-induced T2DM mouse model, a high level of blood glucose was observed. To determine whether HG-induced effects are also involved in 5-HT system activation, D-glucose (33 mM)-stimulated PMHs were treated with or without pCPA and Sar (alone or in combination) to inhibit Tph1 and 5-HT_2R, respectively. As in the PA-treated PMHs, HG led to the activation of the 5-HT system with the upregulation of Tph1, AADC, 5-HT_{2A}R, and 5-HT_{2B}R expression and increased intracellular levels of 5-HT (Fig. 7a). HG also induced ELS and PICG with the activation of PKCε and NF-κB (Fig. 7b) and increased the intracellular levels of TG, H_2O_2, MDA, TNF-α, and IL-1β (Fig. 7c). The inhibitory effects of pCPA and Sar (alone or in combination) were similar to those of siTph1 and si5-$HT_{2A,2B}$R (alone or in combination) in PA-treated HepG2 cells (Fig. 1B), suggesting that HG-induced ELS and PICG are also modulated by the activation of the 5-HT system in PMHs.

T2DM mouse model with NASH correlates with the activation of the hepatic 5-HT system

We found that the levels of dopamine, another molecule synthesized by AADC, were very low and unchanged in the liver and serum of Ctrl and T2DM mice with or without CDP treatment (data not shown), whereas 5-HT levels were significantly elevated in the liver and serum of T2DM mice, and were obviously reduced by CDP treatment; hepatic 5-HT levels were

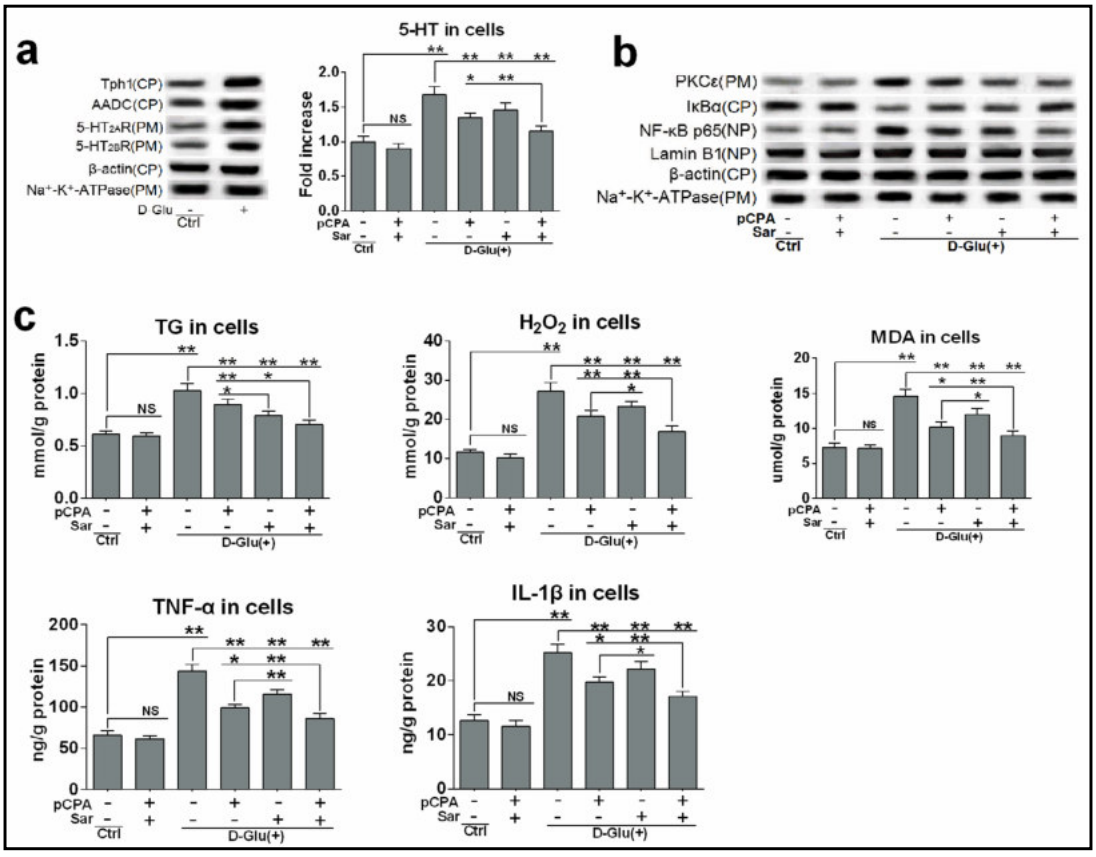

Fig. 7. Relationship between 5-HT system activation and high glucose-induced TG overproduction and PICG in PMHs. PMHs were treated with or without D-Glu (33 mM), treated with either pCPA (30 μM) or Sar (30 μM) and with D-Glu, or co-treated with pCPA and Sar and with or without D-Glu for 6 h (a, b) or 10 h (c). (a, b) Protein levels and 5-HT levels. (c) Levels of TG, H_2O_2, MDA, TNF-α, and IL-1β. Data are presented as the mean ± SD of 3 independent experiments. $^{*}P<0.05$, $^{**}P<0.01$. Abbreviations: NS, not significant; D-Glu, D-glucose; pCPA, para-chlorophenylalanine; Sar, sarpogrelate; CP, cytoplasm; PM, plasmalemma; NP, nucleoplasm.

also inhibited by Sar (Fig. 8a). The expression of hepatic Tph1, AADC, 5-HT_{2A}R, and 5-HT_{2B}R was up-regulated in T2DM mice compared to Ctrl mice (Fig. 8a). T2DM mice exhibited PKCε activation with increased phosphorylation of Akt, mTOR, and ERK1/2, upregulated ACC, GPAT1, and MTTP expression (Fig. 8b), and increased TG and VLDL levels (Fig. 8c) in the liver; they also showed hepatic oxidative stress and inflammation with up-regulated MAO-A expression, increased H_2O_2 and MDA levels, NF-κB activation, increased phosphorylation of p38, JNK, and STAT3, and increased TNF-α and IL-1β levels (Fig. 8b and c). These alterations were remarkably inhibited by Sar and CDP in a synergistic manner.

By hematoxylin and eosin staining (Fig. 8d), we found hepatic steatosis and lobular inflammation with inflammatory cell infiltration and hepatocyte ballooning in the lobes. By Masson's trichrome staining (Fig. 8e), we found hepatic fibrosis in the periportal and parenchymal regions of T2DM mice. These phenotypes were significantly ameliorated by

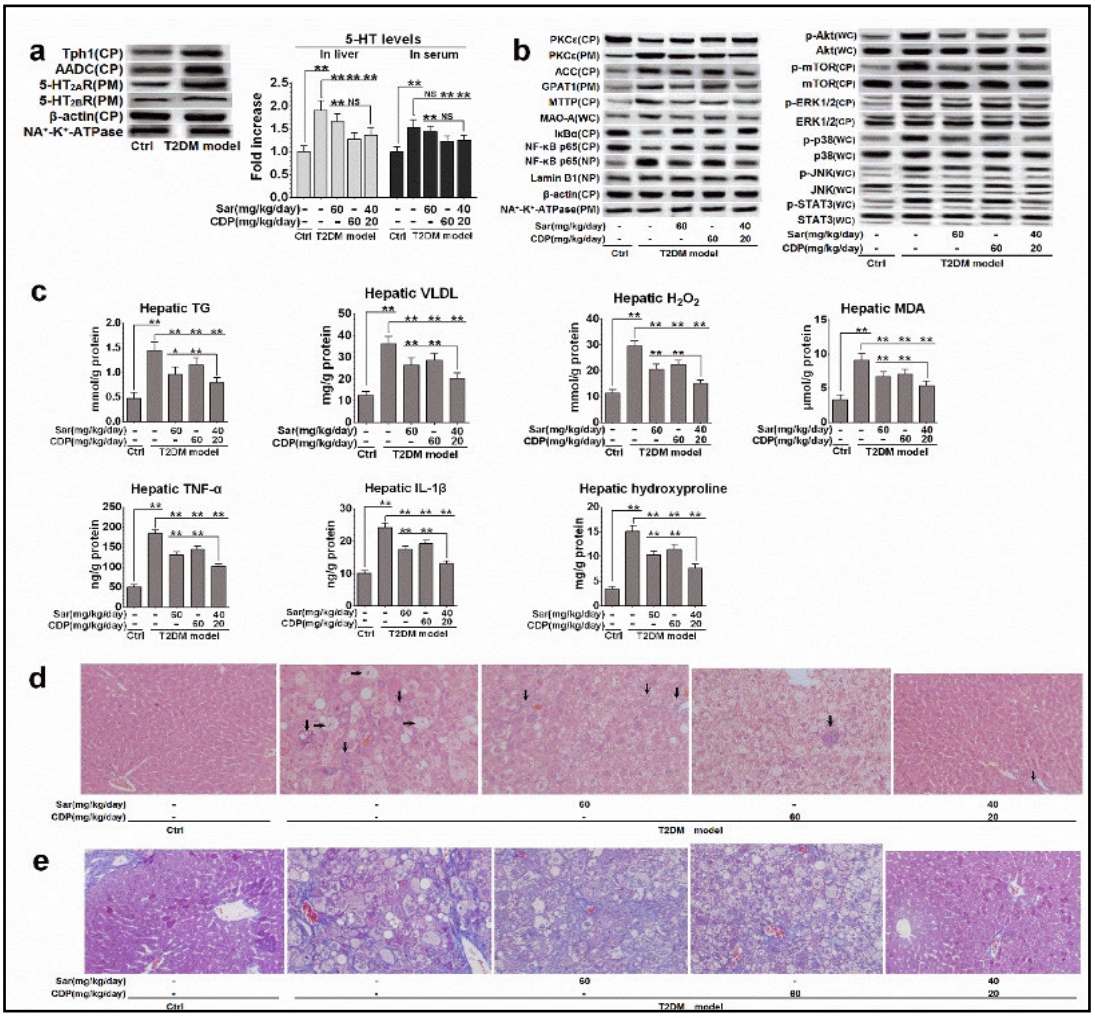

Fig. 8. Therapeutic effects of Sar and CDP on hepatic steatosis, inflammation and fibrosis in the T2DM mouse model. (a, b) Hepatic protein levels and 5-HT levels. (c) Hepatic levels of TG, VLDL, H_2O_2, MDA, TNF-α, IL-1β, and hydroxyproline. (d) By hematoxylin and eosin staining (20×), representative histopathological findings of lipid droplets, inflammatory cells (indicated with vertical arrows), and hepatocyte ballooning (indicated with horizontal arrows). (e) By Masson's trichrome staining (20×), representative hepatic fibrosis findings in the periportal and parenchymal regions. Data are presented as the mean ± SD of 4 mice chosen randomly for the examination of protein expression and of 8 mice for the measurement of the others in each group. $^{*}P<0.05$, $^{**}P<0.01$. Abbreviations: NS, not significant; Sar, sarpogrelate; CDP, carbidopa; CP, cytoplasm; PM, plasmalemma; NP, nucleoplasm; WC, whole cells; p-, phosphorylated.

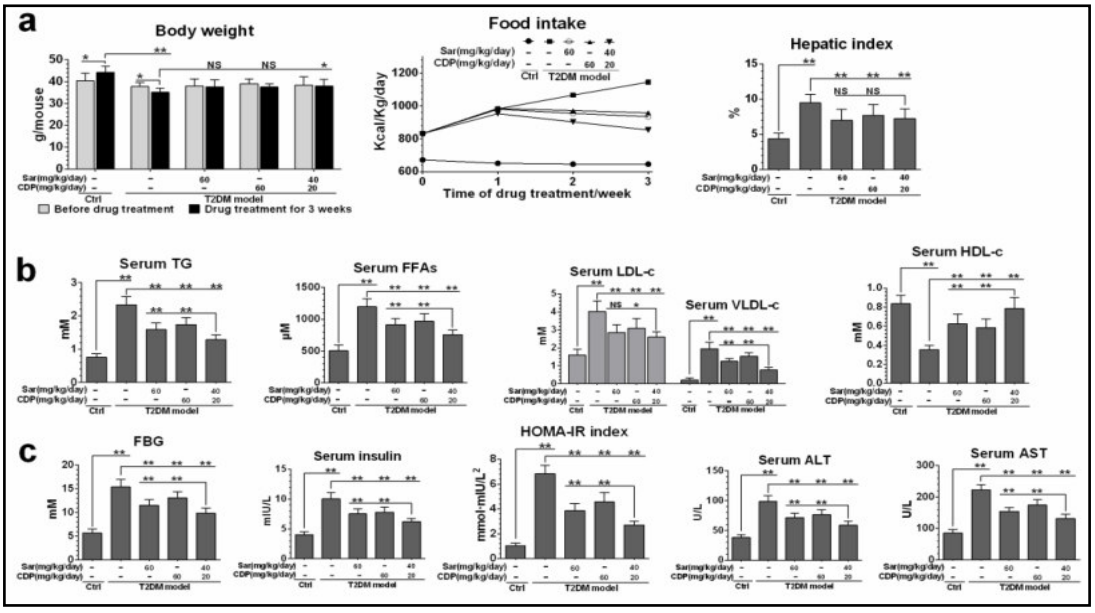

Fig. 9. The effects of Sar and CDP on bodyweight, food intake, hepatic index, and blood factors involved in dyslipidemia, dysglycemia, and liver injury in the T2DM mouse model. (a) Body weight, food intake, and hepatic index; (b) Serum levels of TG, FFAs, LDL-c, VLDL-c, and HDL-c; (c) FBG, serum levels of insulin, and homeostasis model of assessment–IR (HOMA-IR) index, and serum activity of ALT and AST. Data are presented as the mean ± SD of 8 mice in each group. *P<0.05, **P<0.01. Abbreviations: NS, not significant; Sar, sarpogrelate; CDP, carbidopa; FBG, fasting blood glucose.

Sar and CDP, particularly by the combination of both. Additionally, increased hepatic levels of hydroxyproline (Fig. 8c), a marked amino acid in the collagen of fibrous tissue [33], and liver injury with increased activity of serum ALT and AST (Fig. 9c) were also reversed significantly in T2DM mice by Sar and CDP in a synergistic manner.

Treatment with Sar and CDP, alone or in combination, reversed the bodyweight loss and reduced the increases in food intake and hepatic index in T2DM mice (Fig. 9a). Whereas there was no significant difference between the three treatments for the amelioration of bodyweight loss, food intake, and hepatic index, suggesting that these effects are not crucial for treating NASH. Sar and CDP treatment (alone or in combination) of T2DM mice also ameliorated dyslipidemia and IR in a synergistic manner, including a reduction of the increased serum levels of TG, FFAs, LDL-c, and VLDL-c, decreased serum levels of HDL-c (Fig. 9b), and increased levels of fasting blood glucose and serum insulin with an increased HOMA-IR index (Fig. 9c). Taken together, our findings show that 5-HT system activation in the liver is a crucial event leading to T2DM-related NASH.

Discussion

Numerous patients with T2DM develop NAFLD with inflammatory complications, namely, NASH. However, the mechanisms underlying these processes are not understood entirely. We revealed that the 5-HT system, including 5-HT synthesis and 5-HT_2R, is activated in the hepatocytes of a T2DM mouse model, which crucially affected the occurrence of hepatic steatosis and inflammation with fibrosis. 5-HT_2R activation in hepatocytes regulates PKCε activation with the subsequent phosphorylation of Akt, mTOR, and ERK1/2, ultimately resulting in ELS, including *de novo* lipogenesis, and TG and VLDL synthesis with LDA, whereas the activation of both 5-HT synthesis and 5-HT_2R modulates oxidative stress with the activation of NF-κB and inflammatory signaling molecules, including p38, JNK, and STAT3, resulting in PICG.

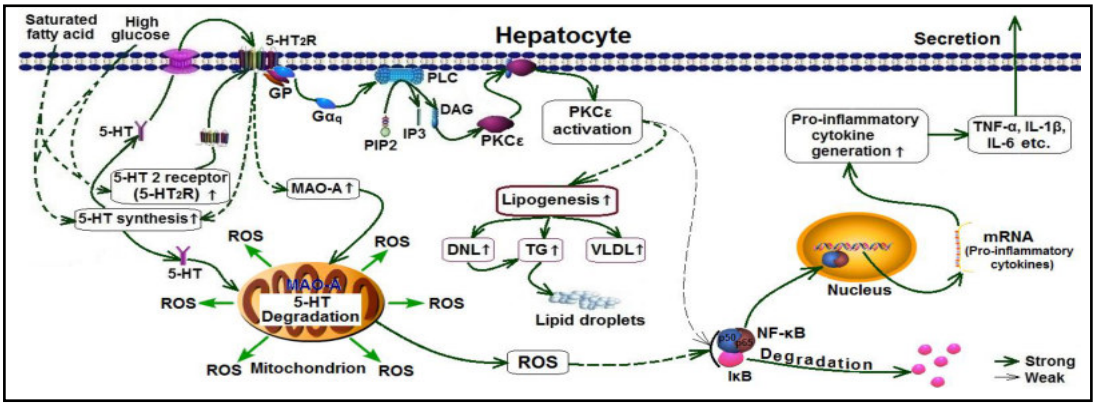

Fig. 10. Mechanisms by which the 5-HT system modulates saturated fatty acid- or high glucose-induced PKCε and NF-κB activation with excessive lipid synthesis and pro-inflammatory cytokine generation in hepatocytes.

In the present understanding, the DAG that initiates PKCε activation originates from TG synthesis in lipid-induced hepatic IR animals [2]. However, this understanding is contentious. Mice in which the lipase activator CGI-58 is knocked down (CGI-58$^{-/-}$) have profound hepatic steatosis, but are protected against HFD-induced hepatic IR [34]. The reason for this protection is the subcellular localization of DAG in liver cells, because these CGI-58$^{-/-}$ mice promote DAG accumulation only in lipid droplets, and not in the cytomembrane, thereby preventing PKCε activation [35]. Studies in humans also showed that the compartmentation of DAG in the cytoplasm and cytomembrane [36, 37] could be an important factor in the pathogenesis of liver and muscle IR, suggesting that only DAG in the cytomembrane has the ability to initiate PKCε activation. No evidence has shown that the DAG located within lipid droplets can be sent to the cytomembrane. According to our results, the origin of the DAG that promotes PKCε activation in PA-treated hepatocytes was via 5-HT$_2$R-coupled G protein G$_q$/PLC pathway activation, which was followed by increased IP3 levels, and not as a result of TG synthesis. In addition, PKCε activation is pivotal but not unique for controlling PA-induced ELS in hepatocytes, as there are other secondary pathways that are also controlled by the 5-HT system to modulate ELS. Furthermore, our results also revealed that PA-induced and 5-HT system-modulated NF-κB activation with PICG has two pathways in hepatocytes: primarily through 5-HT degradation by MAO-A in the mitochondria, to aggravate ROS generation, mainly H_2O_2, leading to oxidative stress, which is also affected by 5-HT$_2$R through controlling 5-HT synthesis and MAO-A expression; and secondarily through PKCε activation. It has been shown that the excessive production of ROS with oxidative stress occurs in the mitochondria of hepatocytes and can lead to NASH with fibrosis [32]. Our results indicated that the origin of these ROS is primarily MAO-A-catalyzed 5-HT degradation in the mitochondria (Fig. 5A). The mechanisms by which the 5-HT system controls diabetes-related dysfunction in hepatocytes are shown in Fig. 10.

The involvement of peripheral 5-HT in the pathogenesis of NASH has been reported [38]: in the choline-methionine-deficient diet-induced steatohepatitis mouse model, 5-HT degradation is an important cause of oxidative stress, and 5-HT-derived ROS modulate mitochondrial damage and lead to hepatocellular injury, which can be treated effectively by knocking down Tph1 (Tph1$^{-/-}$). Peripheral 5-HT is also involved in HFD-induced obesity, IR, and NAFLD, and these effects are clearly prevented in Tph1$^{-/-}$ mice [15]. However, these studies assumed that hepatic 5-HT comes from non-hepatic organs. Our results revealed that hepatic 5-HT originates from its biosynthesis in hepatocytes, and the activation of 5-HT$_2$R, particularly 5-HT$_{2A}$R, is another key factor implicated in the development of NASH. In fact, 5-HT$_2$R activation has been implicated in fibrosis and inflammation in the liver [39], and Sar has also been demonstrated to improve IR in rats with T2DM [16]. Accordingly, we propose that the activation of the 5-HT system, including 5-HT synthesis and 5-HT$_2$R, is an unusual

event in hepatocytes, as an essential "intermediary," which modulates SFA and HG-induced processes of ELS and PICG through the activation of numerous signaling molecules in the liver of patients with T2DM, and the formation of an inflammatory microenvironment in NASH liver, such as high levels of TNF-α, IL-1β, and IL-6.

In further investigations, we need to clarify the systemic role of the 5-HT system and the mechanism by which SFA and HG induce the activation of the 5-HT system in cells. We also observed that treatment with CDP and Sar (alone or in combination) had an indirect inhibitory effect on HFD+STZ-induced NASH as well as directly on the liver, through the reduction of blood glucose and FFA levels with systemic IR. We suggest that targeting the 5-HT system is a potential therapeutic target for T2DM-related NASH with hepatic fibrosis, while a combination of the inhibition of peripheral 5-HT synthesis and $5\text{-HT}_2\text{R}$ is necessary.

Acknowledgements

The authors are grateful to Associate Professor Wenxia Bai (Jiangsu Center for Safety Evaluation of Drugs, China) for her contribution to the histopathological examinations, Professor Lei Qiang (China Pharmaceutical University) and ThinkSCIENCE (Tokyo, Japan) for contribution to language revision of the manuscript, and Shanghai GenePharma Co., Ltd. for designing the lentiviral vector and plasmid vector. This study was supported by the National Natural Science Foundation of China (No. 81570720), Jiangsu Undergraduate Innovation Training Program Fund (No. SY15094), Huahai Pharmaceuticals Graduate Innovation Fund (No. CX13S-003HH), and Postgraduate Research & Practice Innovation Program of Jiangsu Province (No. KYCX17_0723).

Disclosure Statement

All authors report no conflicts of interest.

References

1 Dowman JK, Tomlinson JW, Newsome PN: Systematic review: the diagnosis and staging of non-alcoholic fatty liver disease and non-alcoholic steatohepatitis. Aliment Pharmacol Ther 2011;33:525-540.
2 Perry RJ, Samuel VT, Petersen KF, Shulman GI: The role of hepatic lipids in hepatic insulin resistance and type 2 diabetes. Nature 2014;510:84-91.
3 Cohen JC, Horton JD, Hobbs HH: Human fatty liver disease: old questions and new insights. Science 2011;332:1519-1523.
4 Stefan N, Häring HU: The metabolically benign and malignant fatty liver. Diabetes 2011;60:2011-2017.
5 Gruben N, Shirisverdlov R, Koonen DP, Hofker MH: Nonalcoholic fatty liver disease: A main driver of insulin resistance or a dangerous liaison? Biochim Biophys Acta 2014;1842:2329-2343.
6 Boadle-Biber MC: Regulation of serotonin synthesis. Prog Biophys Mol Biol 1993;60:1-15.
7 Billett EE: Monoamine Oxidase (MAO) in human peripheral tissues. Neurotoxicology 2004;25:139-148.
8 Kato S: Role of serotonin 5-HT3 receptors in intestinal inflammation. Biol Pharm Bull 2013;36:1406-1409.
9 Watts SW, Morrison SF, Davis RP, Barman SM: Serotonin and blood pressure regulation. Pharmacol Rev 2012;64:359-388.
10 Barnes NM, Sharp T: A review of central 5-HT receptors and their function. Neuropharmacology 1999;38:1083-1152.
11 Filip M, Bubar MJ, Cunningham KA: Contribution of serotonin (5-HT) 5-HT 2 receptor subtypes to the discriminative stimulus effects of cocaine in rats. Psychopharmacology 2006;183:482-489.
12 Fu JH, Ma SX, Li X, An SS, Li T, Guo KK, Lin M, Qu W, Wang SS, Dong XY: Long-term stress with hyperglucocorticoidemia-induced hepatic steatosis with VLDL overproduction is dependent on both 5-HT2 receptor and 5-HT synthesis in liver. Int J Biol Sci 2016;12:219-234.

13 Ma SX, Li T, Guo KK, Li X, An SS, Hou SS, Chen R, Yang B, Liu S, Fu JH: Effective treatment with combination of peripheral 5-hydroxytryptamine synthetic inhibitor and 5-hydroxytryptamine 2 receptor antagonist on glucocorticoid-induced whole-body insulin resistance with hyperglycemia. J Diabetes Investig 2016;7:833-844.
14 Li X, Guo KK, Li T, Ma SX, An SS, Wang SS, Di J, He SY, Fu JH: 5-HT 2 receptor mediates high-fat diet-induced hepatic steatosis and very low density lipoprotein overproduction in rats. Obes Res Clin Pract 2016;12:16-28.
15 Crane JD, Palanivel R, Mottillo EP, Bujak AL, Wang H, Ford RJ, Collins A, Blümer RM, Fullerton MD, Yabut JM: Inhibiting peripheral serotonin synthesis reduces obesity and metabolic dysfunction by promoting brown adipose tissue thermogenesis. Nat Med 2015;21:166-172.
16 Takishita E, Takahashi A, Harada N, Yamato M, Yoshizumi M, Nakaya Y: Effect of sarpogrelate hydrochloride, a 5-HT2 blocker, on insulin resistance in Otsuka Long-Evans Tokushima fatty rats (OLETF rats), a type 2 diabetic rat model. J Cardiovasc Pharmacol 2004;43:266-270.
17 Luo J, Quan J, Tsai J, Hobensack CK, Sullivan C, Hector R, Reaven GM: Nongenetic mouse models of non-insulin-dependent diabetes mellitus. Metabolism 1998;47:663-668.
18 Li WC, Ralphs KL, Tosh D: Isolation and culture of adult mouse hepatocytes. Methods Mol Biol 2010;633:185.
19 Dries DR, Gallegos LL, Newton AC: A single residue in the C1 domain sensitizes novel protein kinase C isoforms to cellular diacylglycerol production. J Biol Chem 2007;282:826-830.
20 Liang W, Lindeman JH, Menke AL, Koonen DP, Morrison M, Havekes LM, van den Hoek AM, Kleemann R: Metabolically induced liver inflammation leads to NASH and differs from LPS- or IL-1β-induced chronic inflammation. Lab Invest 2014;94:491-502.
21 Shoelson SE, Lee J, Yuan M: Inflammation and the IKK beta/I kappa B/NF-kappa B axis in obesity- and diet-induced insulin resistance. Int J Obes Relat Metab Disord 2003;27:S49-52.
22 Tak PP, Firestein GS: NF-kappaB: a key role in inflammatory diseases. J Clin Invest 2001;107:7-11.
23 Byrne CD, Targher G: NAFLD: a multisystem disease. J Hepatol 2015;62:S47-64.
24 Diraison F, Moulin P, Beylot M: Contribution of hepatic de novo lipogenesis and reesterification of plasma non esterified fatty acids to plasma triglyceride synthesis during non-alcoholic fatty liver disease. Diabetes Metab 2003;29:478.
25 Hoyer D, Hannon JP, Martin GR: Molecular, pharmacological and functional diversity of 5-HT receptors. Pharmacol Biochem Behav 2002;71:533-554.
26 Macmillan D, Mccarron JG: The phospholipase C inhibitor U-73122 inhibits Ca 2+ release from the intracellular sarcoplasmic reticulum Ca 2+ store by inhibiting Ca 2+ pumps in smooth muscle. Br J Pharmacol 2010;160:1295-1301.
27 Igal RA, Wang P, Coleman RA: Triacsin C blocks de novo synthesis of glycerolipids and cholesterol esters but not recycling of fatty acid into phospholipid: evidence for functionally separate pools of acyl-CoA. Biochem J 1997;324:529-534.
28 Faergeman NJ, Knudsen J: Role of long-chain fatty acyl-CoA esters in the regulation of metabolism and in cell signalling. Biochem J 1997;323:1-12.
29 Karasik A, Rothenberg PL, Yamada K, White MF, Kahn CR: Increased protein kinase C activity is linked to reduced insulin receptor autophosphorylation in liver of starved rats. J Biol Chem 1990;265:10226-10231.
30 Mendoza MC, Er EE, Blenis J: The Ras-ERK and PI3K-mTOR pathways: cross-talk and compensation. Trends Biochem Sci 2011;36:320-328.
31 Johnson JA, Gray MO, Chen CH, Mochly-Rosen D: A protein kinase C translocation inhibitor as an isozyme-selective antagonist of cardiac function. J Biol Chem 1996;271:24962-24966.
32 Tilg H, Moschen AR, Roden M: NAFLD and diabetes mellitus. Nat Rev Gastroenterol Hepatol 2017;14:32-42.
33 Toyoki Y, Sasaki M, Narumi S, Yoshihara S, Morita T, Konn M: Semiquantitative evaluation of hepatic fibrosis by measuring tissue hydroxyproline. Hepatogastroenterology 1998;45:2261-2264.
34 Brown JM, Betters JC, Ma Y, Han X, Yang K, Alger HM, Melchior J, Sawyer J, Shah R, Wilson MD: CGI-58 knockdown in mice causes hepatic steatosis but prevents diet-induced obesity and glucose intolerance. J Lipid Res 2010;51:3306-3315.
35 Cantley JL, Yoshimura T, Camporez JP, Zhang D, Jornayvaz FR, Kumashiro N, Guebre-Egziabher F, Jurczak MJ, Kahn M, Guigni BA: CGI-58 knockdown sequesters diacylglycerols in lipid droplets/ER-preventing diacylglycerol-mediated hepatic insulin resistance. Proc Natl Acad Sci U S A 2013;110:1869-1874.

36 Kumashiro N, Erion DM, Zhang D, Kahn M, Beddow SA, Chu X, Still CD, Gerhard GS, Han X, Dziura J: Cellular mechanism of insulin resistance in nonalcoholic fatty liver disease. Proc Natl Acad Sci U S A 2011;108:16381-16385.

37 Bergman BC, Hunerdosse DM, Kerege A, Playdon MC, Perreault L: Localisation and composition of skeletal muscle diacylglycerol predicts insulin resistance in humans. Diabetologia 2012;55:1140-1150.

38 Nocito A, Dahm F, Jochum W, Jang JH, Georgiev P, Bader M, Renner EL, Clavien PA: Serotonin mediates oxidative stress and mitochondrial toxicity in a murine model of nonalcoholic steatohepatitis. Gastroenterology 2007;133:608-618.

39 Maroteaux L, Aymedietrich E, Aubertinkirch G, Banas S, Quentin E, Lawson R, Monassier L: New therapeutic opportunities for 5-HT2 receptor ligands. Pharmacol Ther 2017;170:14-36.